8 Cryostat

This chapter discusses the design of the LZ cryostat, the extensive program to acquire suitable materials for it, and the simulations of associated backgrounds. The baseline design for the cryostat assumes the use of titanium, although stainless steel is being evaluated as an option. A critical requirement for the cryostat is to limit the contributions to radioactive backgrounds in the sensitive region of the Xe detector. We summarize our simulations of the expected backgrounds from the cryostat in Section 8.1. The results of the R&D program to assay potential cryostat materials are given in Section 8.2. Finally, we described the cryostat design and key interfaces in Section 8.3.

8.1 Background Simulations

The material baseline is commercially pure titanium, Grade 1, due to its low radioactivity, high strength-to-weight ratio, and low density. As a result of these properties, the neutron and gamma absorption in the cryostat is minimized, making it possible to veto backgrounds more efficiently. Titanium of this grade was used successfully for the LUX cryostat [1]. In case we are unable to obtain titanium with the required radiopurity, we are also considering stainless steel (SS) such as SS316L/Ti and SS304L.

The backgrounds have been assessed using the LUXSim [2] code modified to reproduce in detail the design of the LZ detector. Simulation is based on the well-established and validated GEANT4 package [3]. The maximum allowed background for each relevant LZ component is set to be less than 10% of the rate from astrophysical neutrino sources before any S2/S1 rejection. Therefore, the main limitation in terms of background for LZ will be given only by the astrophysical sources (see Chapter 12).

For neutrons, (α,n) reactions and spontaneous fission neutron energy spectra were generated using the SOURCES software [4]. These spectra were then embedded into the LUXSim framework, which propagates neutrons isotropically emitted from the cryostat. For the ^{238}U and ^{232}Th decay chains, we used the approach described in [5], while for the ^{40}K and ^{60}Co decays, we used the standard GEANT4 process [3]. Neutron and gamma yields for Ti and SS are presented in Tables 8.1.1, obtained from [4] and [6], respectively.

Nuclear and electron recoil backgrounds from the cryostat, within the corresponding energy ranges of 1.5-6.5 keV_{ee} and 6-30 keV_{nr}, have been estimated selecting single scatter events in the sensitive LXe volume, assuming radial and horizontal position resolution of 3 and 0.2 cm, respectively. Signals from the LS veto and the LXe TPC skin layer have been used to veto events with energy depositions above 100 keV and within an 800 μs time window. No additional efficiency or S2/S1 cuts have been applied. In the simulation, 5.6 tonnes fiducial mass and 1,000 days' exposure time have been considered, as shown in Figure 3.8.5.1, evaluated after all the veto systems are applied.

The "Maximum Allowed Radioactivity (mBq/kg)," shown in Table 8.1.2, indicates the radioactivity from

Table 8.1.1. Neutron and gamma rates in the background simulation described in the text.

	Titanium	Stainless Steel
	Neutron Yield (10^{-6} n/s at 1 Bq/kg)	
U	3.1	1.5
Th	5.3	1.4
	Gamma Yield (gamma/decay)	
U	2.23	
Th	2.74	
K	0.1	
Co	2	

Table 8.1.2. Results from cryostat gamma background simulations for titanium and stainless steel.

Maximum Allowed Radioactivity [mBq/kg]		
	Titanium	**Stainless Steel**
^{238}U	0.75	0.67
^{232}Th	0.51	0.74
^{40}K	16.81	8.50
^{60}Co	-	2.28

each isotope — ^{238}U, ^{232}Th, ^{40}K, and ^{60}Co — that corresponds in total to one-third of 10% of the background from the astrophysical pp neutrinos (ER) and nuclear scattering (NR).

We have considered the Ti assay results by LZ, detailed in Section 8.2, and the SS considered for the Neutrino Experiment with a Xenon TPC (NEXT) collaboration [7] and our own results, also described in Section 8.2. Results for Ti from TIMET [8] and potentially also SS show that these materials would satisfy the allowed activity for the fiducial mass of 5.6 tonnes. Titanium has lower backgrounds, as described below, and is our preferred choice.

8.2 Cryostat Material Searches

The baseline design is to use CP-1-grade Ti for the inner and outer vessels of the cryostat for LZ, due to its low radiological background content. The Ti used in LUX contains <0.25 mBq/kg of ^{238}U, <0.2 mBq/kg of ^{232}Th, and <1.2 mBq/kg of ^{40}K; however, such low values appear to be rare, and readily procuring Ti with similar levels of contaminants has proved difficult for several other experiments. LZ groups at Rutherford Appleton Laboratory (RAL) and University College London (UCL) have embarked on a program of R&D, working with partners from the Ti production industry, to identify the points of inclusion of contamination during the Ti roll stock manufacturing processes, to control their effect, and to procure sufficiently clean material — with contamination levels comparable to the LUX Ti.

The production of Ti metal is a complex procedure that involves a number of stages in which additives and inclusions are deliberately introduced. Several such points in the production cycle may contribute to contamination of the final metal with elements containing radioactive isotopes; ^{238}U, ^{235}U, and ^{232}Th are of particular concern. The refinement of the mineral concentrates, particularly for ilmenite, involves the addition of or exposure to coke, coal, oil, and tar prior to the chlorination process. It is not uncommon for such materials to contain relatively high levels of U and Th. However, the $TiCl_4$ produced at this stage undergoes chemical treatment and filtering to remove chlorides and sludge before pure liquid $TiCl_4$ is created, carrying away most impurities, including U and Th. Ultrapure $TiCl_4$ is commercially available, as are titanium hydride and titanium nitride powders that are produced through plasmochemical processing from the $TiCl_4$. Beyond this stage, lack of sufficient contact controls with surfaces during the Kroll process and metallothermy present other potential sources of U and Th. However, the elements introduced — largely Mg and Ar — will probably not be problematic. The Ti sponge post-Kroll processing is exposed to several stages in which U and Th can enter the chain. Ti ingots and slabs are produced by pressing and melting the Ti sponge, yet often Ti alloy and Ti scrap is added at this stage. Other alloys such as aluminum and vanadium may also be included. Radioactive contamination contained within the scrap and alloys is then carried through to the Ti ingot and into the roll stock. The major stages of this production process, indicating inclusion points, are depicted in Figure 8.2.1 [9].

During this R&D period we have engaged several titanium providers including VSMPO [10], TIMET Supra Alloy [11], Honeywell [12], and PTG [13] to provide sample material, taken from various stages along the production process, in order to determine where radioactivity, particularly U and Th, enters the

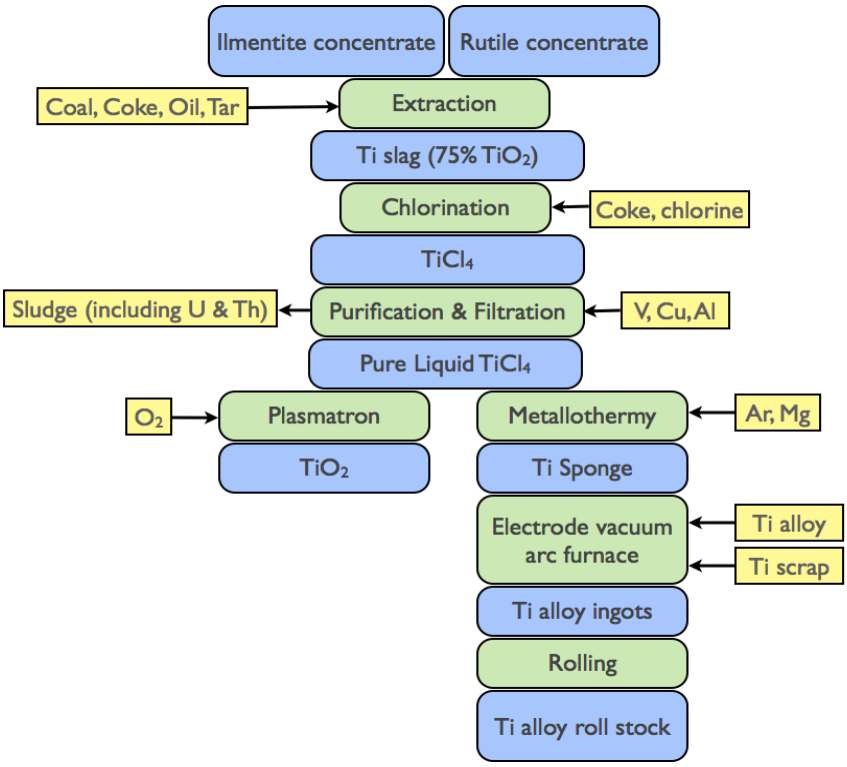

Figure 8.2.1. The commercial production of Ti metal, indicating the major stages (green boxes), the post-processing products (blue boxes), and the additives, as well as reductions during the procedure (yellow boxes). Figure adapted from [9].

chain. In our campaign we have received 22 samples including: eight sponges, one sample of very-high-purity Ti (Honeywell), one Grade-1 with 10% scrap (VSMPO), two Grade-2 sheets (Supra Alloy and PTG), eight Grade-1 sheets (Supra Alloy, PTG and TIMET) — and also Ti bolts and nuts.

Table 8.2.1 summarizes all the Ti samples that have been radioassayed in this campaign. Results from the LUX material campaign are included for comparison. We note that sample #22 in Table 8.2.1 represents the lowest radio-impurity contamination ever reported for a titanium sample, with activities of <1.6/<0.09 mBq/kg for U_e /U_l and also 0.28/0.23 mBq/kg for Th_e/Th_l, respectively.

Low-background experiments searching for dark matter or neutrinoless double-beta decay, such as XENON-1T [14] and PANDA-X [15], or GERDA [16] and NEXT, respectively, use stainless steel for their cryostats, with the majority of materials coming from German stockholder NIRONIT [17]. We procured 13 samples from NIRONIT for radioassay. We also conducted independent assays of samples received directly from the GERDA and NEXT experiments, to cross-check published results [7-18] and to measure radioisotopes not reported, as well as early U and Th activity.

The 13 SS samples were received in November 2014 (a total of 152 kg). They originate from different heats and were made by different mills: seven samples at TyssenKrup Nirosta (Germany) and six samples at Aperam (Belgium). All samples were electropolished at LBNL and prescreened with a surface HPGe counter (MERLIN), particularly for excessive ^{60}Co. Samples with <20 mBq/kg of ^{60}Co were forwarded for more sensitive tests underground at SURF and at the University of Alabama. Stainless steel radioassays are summarized in Table 8.2.2.

An impact of the titanium from TIMET and stainless steel from NIRONIT on LZ background is presented in Figure 12.3.3.1.

Table 8.2.1. Summary of the 22 samples assayed for the LZ cryostat, including various grades and types from multiple suppliers.

#	Supplier	Sample name	238U (mBq/kg)		232Th (mBq/kg)		40K (mBq/kg)	Ti grade/type	Report Date
			early	late	early	late			
1	Supra Alloy	Carlson 8J102	31.00	4.10	0	2.80	*1.80*	CP-1 Sheet	Jan 2013
2	TIMET	Osaka 26-29461	*2.50*	248	0	*4.10*	*12.00*	Sponge	Aug 2013
3	TIMET	Tangshan TX027594	*2.50*	6200	0	*2.50*	*15.00*	Sponge	Aug 2013
4	TIMET	Toho C 12009C	*2.50*	*62*	0	*1.60*	*12.10*	Sponge	Aug 2013
5	TIMET	TOHO W 11266W	*2.50*	124	0	*1.60*	*12.00*	Sponge	Aug 2013
6	TIMET	Zaporozhye 6680-12	*2.50*	744	0	*1.60*	*12.00*	Sponge	Aug 2013
7	TIMET	ZUNY TX027641	25.00	2480	0	4.1	*12.0*	Sponge	Aug 2013
8	TIMET	HN0021-B sample1	11.00	*0.60*	0	*0.60*	*2.50*	CP-1 Sheet	Aug 2013
9	TIMET	HN0021-B sample 2	4.90	3.33	2.85	0.80	*1.50*	CP-1 Sheet	Sept 2013
10	PTG	ATI W74M	46.00	2.80	0	2.80	*1.80*	CP-1 Sheet	Jan 2013
11	Supra Alloy	Timet BN3672(2) RMI 404666 (9)	110.00	*2.40*	0	170.00	2.40	CP-2	Jan 2013
12	PTG	Thyssen Krupp 611292	*9.60*	3.60	0	2.40	*2.10*	CP-2	Jan 2013
13	TIMET	Henderson 22-49312	*3.70*	2480	0	12.30	*18.00*	Sponge	Aug 2013
14	S6MB annulus	Bolts	1300.00	*6.00*	0	160.00	*60.00*	Bolts	Jan 2013
15	EE-33 full	Nuts	500.00	*8.40*	0	80.00	*60.00*	Nuts	Jan 2013
16	Honeywell	T149858991	3.70	4.69	0	1.63	*1.50*	CP-1 Sheet	Sept 2013
17	VSMPO	528 g	*61.70*	*6.20*	0	*4.10*	*31.00*	CP-1 Metal (10% scrap)	Jan 14
18	VSMPO	996 g	17.28	12.35	0	*4.10*	*6.20*	CP-1 Sponge	Jan14
20	TIMET	HN2470	8.51	0.37	0	0.61	0.52	CP-1 Sheet	Nov 14
21	TIMET	Master ID #46	8.00	*0.124*	0	*0.12*	*0.62*	CP-1 Sheet	Sept 14
22	TIMET	HN3469	*1.60*	*0.09*	0.28	0.23	*0.54*	CP-1 slab	Jun-16

Table 8.2.2. Summary of the 13 stainless steel samples radioassayed for LZ. Due to a high ^{60}Co content detected in samples 10-13 during prescreening, these were not assayed further and as such early-chain contents were not measured (the prescreen detector is not sensitive to early-chain decays).

#	Sample name	238U (mBq/kg)		232Th (mBq/kg)		60Co (mBq/kg)	40K (mBq/kg)
		early	late	early	late		
1	NIRONIT 311113	7.3	0.35	1.1	4	14.5	*0.53*
2	NIRONIT 511803	1.2	0.27	0.33	0.49	1.6	*0.4*
3	NIRONIT 512006	*1*	0.54	0.49	1.1	1.7	*0.59*
4	NIRONIT 512844	1.4	0.5	0.5	0.32	2.6	*0.5*
5	NIRONIT 521663	1.9	0.38	0.81	0.73	5.6	*0.46*
6	NIRONIT 521994	0.5	1.9	1.7	1.5	4.5	*0.5*
7	NIRONIT 124113	0	1.1	0	4.1	8.2	*3*
	NIRONIT (Alab) 124113	0+/-22	4.89	0	5.37	14.6	1.7
8	NIRONIT 211093	0	*0.6*	0	*0.8*	7.4	*3*
	NIRONIT (Alab) 211093	0+/-11	2.46	0	0.37	14	0
9	NIRONIT 528292	0	*0.6*	0	*0.9*	6.5	*3*
	NIRONIT (Alab) 528292	0+/-22	2.22	0	0.67	9.69	0
10	NIRONIT 832090	0	4	0	2.2	26	*4*
11	NIRONIT 407156	0	*0.6*	0	4.8	32	*2*
12	NIRONIT 528194	0	*0.8*	0	2.1	32	5
13	NIRONIT 828660	0	*1.4*	0	*1.5*	335	*4*

We have determined that the highest radiopurity is achieved using a combination of commercially pure titanium (0.03% N, 0.1% C, 0.015% H, 0.2% Fe, 0.18% O, 99.475% Ti as per ASTM B265 required by the ASME BPVC) without added scrap material and cold hearth electron beam (EB) refining technology ("EB melting"). Cold hearth melting provides an important mechanism by which high-density contaminants are removed by gravity separation and settle in the cold hearth. By contrast, vacuum arc remelting (VAR) technology provides virtually no refining of the raw material. These two factors — no scrap and EB melting — are the key elements in the titanium production that assure a low level of radioactive contamination.

8.3 Cryostat Design

8.3.1 Material, Working, and Transportation Conditions

The baseline material for the LZ cryostat is commercially pure Ti, Grade 1 per ASME SB-265, with additional low-radioactivity background requirements as presented above. The design of the vessels complies with the following codes: ASME BPVC [19], 2012 Int. Building Code, and ASCE 7, with site soil classification Class B (Rock) for seismic conditions. The 2008 U.S. Geological Survey hazard data [20] for this location are: S_S = 0.121 g, S_{MS} = 0.121 g, and S_{DS} = 0.081 g. The Seismic Design Force for LZ is 0.054g, which imposes a force of 5297 N at the center of mass of the cryostat during an event. The outer-vessel support and base fasteners are adequate to withstand this force; the inner-vessel tie rod supports need careful consideration when taking this force into account. A combination of reaction points will be incorporated into the vessel design to react to the vertical and horizontal forces.

The assembly of the cryostat underground assumes that the inner vessel along with its contents will be moved as an assembly down the Yates shaft at SURF. The width of the shaft is nominally 1.85 m, and the maximum payload width is 1.70 m to clear features in the shaft cross section and provide some margin of safety. The outer vessel may be moved down the Yates shaft in pieces.

The LZ cryostat operational temperatures (°C) and pressures (bar absolute) are summarized in Table 8.3.1.1.

Table 8.3.1.1. Pressures and temperatures for cryostat operational conditions: normal, bakeout, and most severe failures.

Vessel	Pressure (bar absolute)		Temperature (°C)	Condition
	Internal	External		
Inner	≤ 4.0	Vacuum	-112 to 37	Normal
	Vacuum	1.01	≤ 100	Bakeout (dry, no water in water tank)
	Vacuum	1.48	-112 to 37	Failure Mode (water flooded between inner and outer vessels)
Outer	Vacuum	1.48	0 to 37	Normal
	Vacuum	1.01	≤ 100	Bakeout (dry, no water in water tank)
	1.48	1.01	0 to 37	Failure Mode (Xe gas leak between inner and outer vessels and no water in water tank)

8.3.2 Baseline Vessel Design

The baseline vessel design is a conventional cylindrical geometry with ellipsoidal heads, as shown in Figure 8.3.2.1. The inner vessel is split once near the top head with a flange pair. To minimize the passive

volume filled with LXe, the diameter of the inner vessel is tapered at its half-height and the bottom head has an ellipsoidal shape with a 3:1 aspect ratio (the other three heads have 2:1 aspect ratios).

To comply with ASME code, a stiffening ring has been located at the smaller aperture of the conical section of the inner vessel. This ring acts as a support line and therefore allows a thinner wall of the top section of the vessel, which can be reduced, i.e., from 8 to 6 mm. The outer vessel is split twice, once near the top head and again in midsection. Because the inner vessel is making full use of the Yates shaft cross section, it is impossible for the outer vessel to be conveyed together. With a three-piece design, the outer vessel can be transported down the Yates shaft in pieces and reassembled once in the Davis Cavern. Considerable thought was put into finishing fabrication of the outer vessel underground, but this idea was dropped in favor of adding a second flange pair. Welding and pressure-testing underground would add unnecessary schedule risk to the project.

For internal pressure, the thickness of the vessel walls in the cylindrical section is governed by a

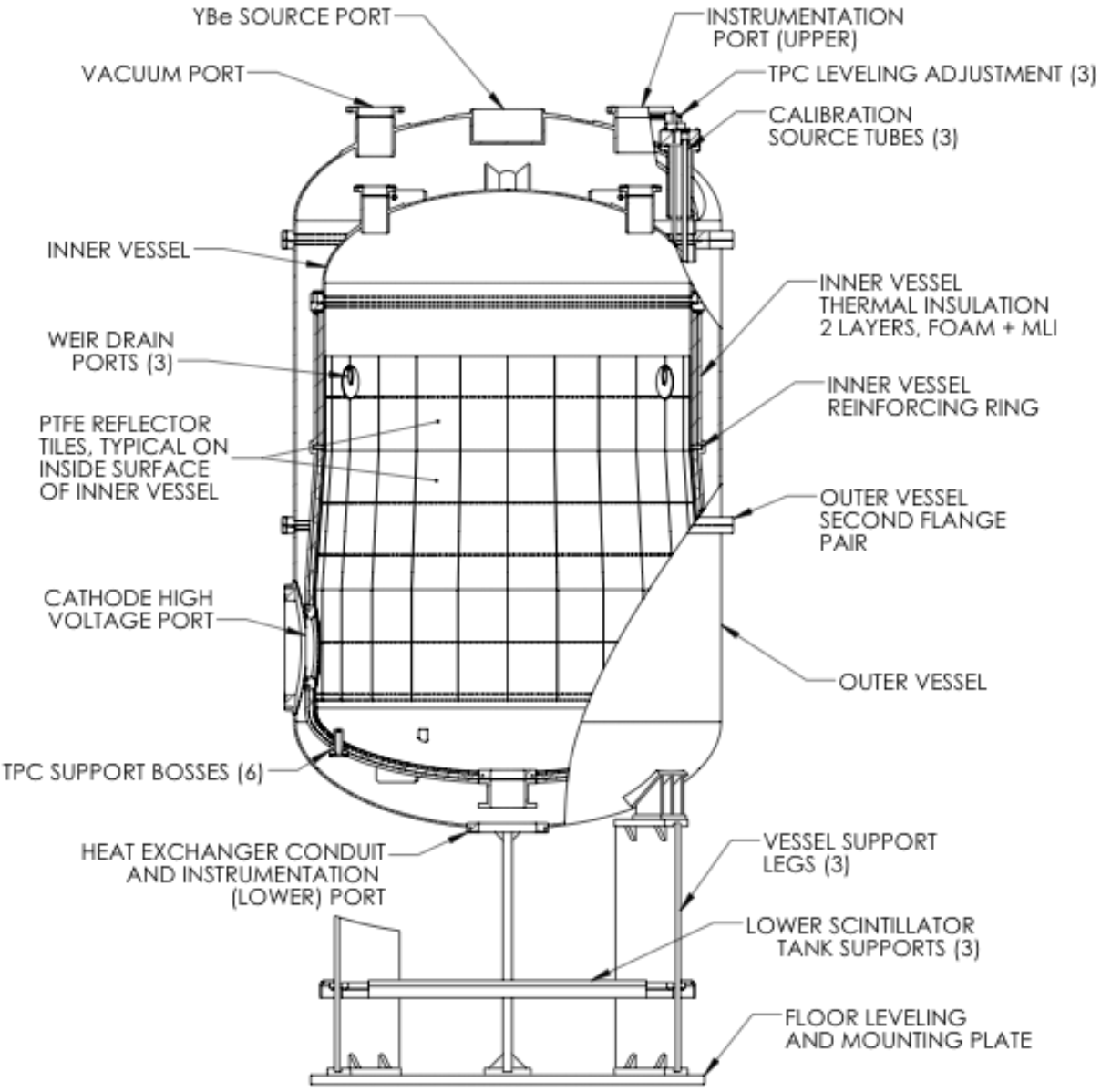

Figure 8.3.2.1. View of the LZ cryostat. Main parts of the inner and outer vessel assembly are highlighted.

Table 8.3.2.1. Minimum wall thickness based on internal pressure and materials considered for the LZ cryostat.

Material	Inner Vessel Wall Thickness (mm)
Ti, CP, Grade 1 (baseline)	5.5
Cu103	8.2
SS316L	3.3

straightforward formula in the pressure vessel code. The minimum wall thickness is a function of the material, vessel diameter, pressure, and degree of inspection. Three materials were considered for this experiment. At the required internal pressure, the minimum wall thicknesses in the cylindrical section are listed in Table 8.3.2.1.

A number of ports are necessary to carry fluids and electrical signals to and from the inner detector. These are added to the top and bottom heads, as well as a side penetration for cathode HV. The latter is discussed in a separate section of Chapter 6.

Buckling is an important failure mode to consider for vessels that see external pressure (vacuum in this case). The ASME BPVC specifies safe external working pressures based on material, temperature, wall thickness, diameter, and length. If the allowable external pressure is insufficient, a vessel designer has a couple of options. The first is to increase the wall thickness. In the case of LZ, this is undesirable for a number of reasons: Most notably, it creates more background radiation and reduces veto efficiency. The other option is to add reinforcing rings. Reinforcing rings essentially shorten the length of the vessel from a buckling perspective. Because the outer vessel is already segmented for transportation reasons, this makes a natural reinforcement against buckling.

Comparing the values for internal pressure 4 bar versus external pressure 1.48 bar, it is evident that the vessel design is driven by external pressure. It should also be noted that the minimum wall thickness is the minimum as-built, not the nominal. During the head-forming process, for instance, flat material is drawn or spun into shape, and in that process thinned from its original thickness. It should also be remembered that material is commercially available in discrete increments as opposed to infinitely variable thickness. Total mass and minimum thicknesses required by the ASME code for each segment of the inner and outer vessel made of Ti and SS are summarized in Table 8.3.2.2

To minimize the amount of LXe between the TPC and the inner cryostat, the shape of the inner vessel is tapered at its half-height. Studies of the electric-field distribution show that the electric field is below the maximum allowed value of 50 kV/cm.

The outer vessel will be sealed (twice, since there are two flange pairs) with differentially pumped double Viton O-rings. This is the most reliable and cost-effective sealing solution for this large room-temperature application. The inner vessel will be sealed with a sprung metal C-seal because at the experimental temperature, O-ring seals with typical elastomeric materials are not suitable. Additionally, the large diameter prohibits the use of a knife-edge flange. Smaller ports on the vessels will be sealed with either a

Table 8.3.2.2. Vessel-wall thicknesses (mm) and total mass (kg) imposed by the external pressure at the normal, bakeout, and failure conditions.

	Inner Vessel						Outer Vessel			
Material	**Top head (mm)**	**Upper wall (mm)**	**Conical section (mm)**	**Lower wall (mm)**	**Dished end (mm)**	**Total mass (kg)**	**Top head (mm)**	**Wall (mm)**	**Dished end (mm)**	**Total mass (kg)**
Titanium	8	6	8	8	12	736	8	8	8	1091
SS316L	6	5	6	6	9	1033	7	7	7	1844

sprung metal C-seal or traditional knife-edge flange. Commercially pure Ti itself is too soft to support a knife-edge feature, but the smaller ports can make use of readily available explosion bonded flanges that feature an SS face and Ti back.

Inner-vessel flanges with knife-edge or C-seal gaskets for cryogenic service will also feature a secondary O-ring seal to facilitate room-temperature leak detection.

8.3.3 Leveling System

Leveling will be done in two stages, with a different degree of precision required for each. The first stage entails surveying and shimming of the outer vessel to level it to on the order of 1:1000. This will be done during installation of the outer vessel and its support legs or base. At this time, it will be convenient to add shims between the legs and the bottom of the water tank, or between the legs and the bottom of the outer vessel. All of the parts above will be manufactured nominally parallel, but obviously there will be some manufacturing variation to mitigate in order to get the gate and anode grids parallel to the liquid/gas interface. Additionally, the result of hydrostatic forces and thermal contraction on the internal parts means that some fine-tuning of the level will be required after the vessel is cooled and filled with LXe, despite a best effort on the assembly when warm and dry. For this second leveling stage, an adjustable three-point suspension system will be used to fine-tune the level of the inner cryostat en masse, much like the method used successfully in LUX.

The LZ suspension rods feature a double bellows seal for both reliability and compliance with the as-built geometry of the vessels. The suspension system is accessible through the water and outer-detector veto tanks. The suspension rods are long enough, and small enough in diameter, to prevent significant heat transfer via conduction. A conceptual model of the suspension is shown in Figure 8.3.3.1.

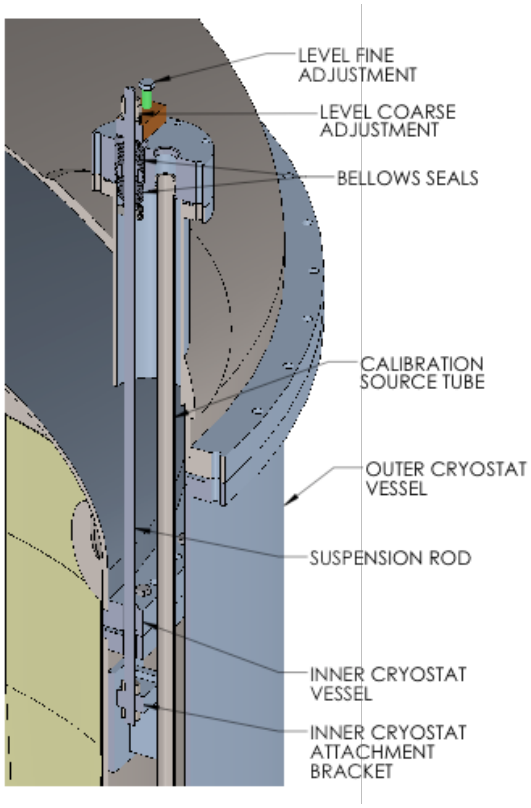

Figure 8.3.3.1. Model of the suspension system for the inner vessel leveling.

8.3.4 Calibration Tubes

Calibration tubes surround the detector in three vertical locations, allowing suitable scans of the TPC with external sealed sources. Titanium (CP-1) or oxygen-free-copper fabricated calibration tubes are equally spaced and straddled across the HV port, and reside in the vacuum space between the inner and outer vessels of the cryostat (see Figures 8.3.2.1 and 8.3.3.1). The calibration source tube enters the vacuum space via a sealing boss directly above the tubes, on the outer vessel dished head, ensuring source delivery simplicity. The source tubes run vertically from the top of the outer vessel dished head to the bottom of the TPC. The size of the source tubes has been optimized to allow use of many types of calibration sources, i.e., AmBe, small neutron generator, or gamma sources. The source tubes are evacuated to avoid further radon contamination.

8.3.5 Cathode High-voltage Port for the Inner and Outer Vessel

The HV port provides an interface for the HV connection and the TPC. The inner-vessel port design must be able to sustain a local field strength of up to 50 kV/cm. Both inner- and outer-vessel ports are manufactured from the vessel parent material and will require soft-metal sealing technology in the form

of a sprung C-seal operating at better than 10^{-9} mbar·l/s. The detector vessel supports one 254-mm-inner-diameter HV port with a suitable flange arrangement and a large aperture for the outer vessel, enabling installation of the vacuum jacket (VJ), promoting ease of assembly, and ensuring integrity of seals, as shown in Figure 8.3.2.1. Both ports are designed to ASME BVPC, Division 1, and will be made from a single metal block using a computer-controlled milling machine.

8.3.6 Cryostat Base

The cryostat base supports the mass of the cryostat and the TPC and also provides a point of attachment to the water-tank floor, thus overcoming any buoyancy effects. The base is attached to the pre-aligned mounting plate, which is anchored to the floor, according to the local civil engineering requirements. This mounting plate defines the apparatus datum; all subsequent surveys will refer to the center point, X:0,Y:0,Z:0. As shown in Figure 8.3.2.1, the support base comprises a three-fin leg design with cross braces, minimizing the number of lower veto tanks required, and providing greater veto efficiency and reduced cost. Veto tanks rest and clamp to a structural support shelf. The base is leveled with respect to the ground mounting plate, and fine adjustments are made by shim plates at the base vessel interface; hence, the cryostat is aligned correctly.

8.3.7 TPC Support Bosses

The interface between the TPC and inner vessel will be six bosses on the bottom head of the inner vessel, as shown in Figure 8.3.2.1. The lower PMT array mounting plate will have mating features that will include a lead-in feature and nut plates so that when the TPC assembly is lowered into the inner vessel, screws can be inserted through the outside bottom head of the inner vessel to secure the TPC assembly. After securing the TPC, the bosses, which from the outside are essentially small ports, will be blanked off in the same manner as all round ports on the vessels. The mating surface of the bosses and the screw holes will be machined after welding to the bottom head to provide the most accurate interface, and to keep them concentric with the inner vessel, mutually co-planar, and perpendicular to the inner vessel axis.

The load on these bosses varies at different stages of assembly, transportation, and operation. During assembly, the load is vertical and in compression; during underground transportation with a horizontal vessel axis, the bosses are designed to handle the shear loads and movement of a horizontal TPC (supports at the top of the TPC ensure that the TPC is not entirely cantilevered off these bottom bosses). In operation, the load is again vertical but this time in tension, as the TPC is buoyant in the very dense LXe. The load and the resulting stress in the bottom head during operation are dominated by pressure, not the TPC bosses. The bosses are far enough away from the highest stress area of the bottom head "knuckle" to be of little consequence.

8.3.8 PTFE Reflector Coating

Photomultiplier tubes (PMTs) in the skin region (outside the TPC but inside the inner vessel) are part of the LZ veto strategy. Polytetrafluoroethylene (PTFE) is required on the inside surfaces of the inner vessel to efficiently reflect light generated by the scintillation of LXe in this skin region. Without PTFE, light that strikes the walls of the inner vessel would be absorbed and never reach the PMTs to be counted.

PTFE is used very successfully as a reflective material in LUX, and no other dielectric material is known to be as efficient in the VUV. Several other polymers in the Teflon "family," ETFE (ethylene tetrafluoroethylene) and PFA (perfluoroalkoxy), for instance, would be desirable because of their manufacturing properties but these materials are not yet proven for this application. It would be very convenient, for instance, to coat the inner vessel in the manner of typical household cookware, but this method is not possible with PTFE, and the resulting coating is too thin. Crucially, small dielectric particles must be avoided at all cost near HV areas of the TPC, and therefore a thicker PTFE material is preferred. It has been shown that thicker films, of order of millimeters rather than micrometers, are required for maximum VUV reflectivity [21]. PTFE has a coefficient of thermal expansion that is an order of magnitude greater than typical metals. The material shrinks approximately 1.45%, going from

room temperature to the working temperature in the detector. A 1.5-m part would therefore shrink about 2 cm on cooldown, so if the PTFE lining in the vessel was a continuous part, it would pull away substantially (about 1 cm radially) from the walls of the vessel when cooling. With this in mind, the only way to mitigate the difference in thermal expansion is to tile the inside surfaces of the vessel with discrete parts that overlap. Individual tiles would be attached with a Teflon central screw, and in cases where the tile is substantially rectangular as opposed to square, there would be a central screw with a round hole and a second screw with a slotted feature in the tile. The Teflon screws would thread into nut plates welded to the inner surface of the vessel wall. An example of this concept is shown in Figure 8.3.2.1.

8.3.9 Thermal Insulation

It is important to limit the heat transfer between the inner vessel and the environment to minimize the amount of refrigeration needed underground. In addition, reducing heat transfer helps to prevent unwanted convection currents in the LXe fluid. The vacuum between nested inner and outer vessels essentially eliminates thermal conduction and convection, in typical Dewar fashion. The dominant mode of heat transfer is therefore radiation, and with a large surface area (~16 square meters) and a large temperature difference, it is potentially substantial. Multilayer insulation (MLI or superinsulation) is proposed as the baseline solution to reduce this thermal load during normal operation. MLI is a well-known insulating material for in-vacuum cryogenic service. The thermal load with and without this material varies by approximately an order of magnitude. In this case, the expected heat load with bare vessels would be several hundred watts, and with MLI several tens of watts. In this experiment, the proposed amount of total refrigeration is about a kilowatt, so MLI is the clear choice.

MLI works well during normal operation, but is ineffective in the event of a failure in which a gross amount of liquid water enters the volume normally occupied by vacuum between the vessels. To mitigate this failure mode, a closed-cell polyurethane foam will be applied to the outer surface of the inner vessel anywhere it is in contact with LXe (basically everywhere below the main seal flange). The proposed foam thickness is 2 cm over the bottom head, and 1 cm over the remainder. MLI will be wrapped over the foam, and covers the entire inner vessel and its cold appendages. With the foam in place, the maximum heat transfer in this failure mode is expected to be 3600 W, which corresponds to a Xe boil-off of 450 standard liters per minute (slpm). This rate is within the Xe-recovery capacity of the system.

Chapter 8 References

[1] D. S. Akerib *et al.* (LUX), "Radio-assay of Titanium samples for the LUX Experiment," (2011), arXiv:1112.1376 [physics.ins-det].

[2] D. S. Akerib *et al.* (LUX), Nucl. Instrum. Meth. **A675**, 63 (2012), arXiv:1111.2074 [physics.data-an].

[3] S. Agostinelli *et al.* (GEANT4), Nucl. Instrum. Meth. **A506**, 250 (2003).

[4] W. B. Wilson, R. T. Perry, W. S. Charlton, and T. A. Parish, Prog. Nucl. Energy **51**, 608 (2009), (SOURCES-4C).

[5] K. Kazkaz and N. Walsh, Nucl. Instrum. Meth. **A654**, 170 (2011), arXiv:1104.2834 [nucl-ex].

[6] *The WISE Uranium Project Calculators!*, WISE Uranium Project, Peter Diehl, Am Schwedenteich 4, 01477 Arnsdorf, Germany (2015).

[7] V. Álvarez *et al.* (NEXT), J. Instrum. **8**, T01002 (2013), arXiv:1211.3961 [physics.ins-det].

[8] (2015), TIMET, 224 Valley Creek Blvd. Suite 200, Exton, PA 19341-2300.

[9] A. Chepurnov, S. Nisi, M. L. di Vacri, and Y. Suvorov, in *LOW RADIOACTIVITY TECHNIQUES 2013 (LRT 2013): Proceedings of the IV International Workshop in Low Radioactivity Technique*, AIP Conf. Proc., Vol. **1549**, edited by L. Miramonti and L. Pandola (2013) pp. 161–164, *The ultra-pure Ti for the low background experiments*, Conference Presentation; E. Mozhevitina, A. Chepurnov, A. Chub, I. Avetissov, V. Glebovsky, S. Nisi, M. L. d. Vacri, and Y. Suvorov, in *Low Radioactivity Techniques 2015 (LRT 2015): Proceedings of the 5th International Workshop in Low Radioactivity Techniques*, AIP Conf. Proc., Vol. **1672** (2015) p. 050001, *Study of the Kroll-process to produce ultra-pure Ti for the low background experiments*, Conference Presentation.

[10] (2015), VSMPO-AVISMA, Parkovaya St. 1, Verkhnaya Salda, Sverdlovsk Region, 624760, Russia.

[11] (2015), Supra Alloys, 351 Cortez Circle, Camarillo, CA 93012-8638, USA.

[12] (2015), Honeywell Electronic Materials, 15128 E Euclid Ave, Spokane Valley, WA 99216-1801, USA.

[13] (2015), PTG - Performance Titanium Group, 8400 Miramar Rd Suite 200-248C San Diego, CA 92126-4387, USA.

[14] E. Aprile (XENON1T), in *Proceedings, 10th UCLA Symposium on Sources and Detection of Dark Matter and Dark Energy in the Universe*, Springer Proc. Phys., Vol. **148** (2013) pp. 93–96, *The XENON1T Dark Matter Search Experiment*, Conference Presentation, arXiv:1206.6288 [astro-ph].

[15] X. Cao *et al.* (PandaX-I), Sci. China Phys. Mech. Astron. **57**, 1476 (2014), arXiv:1405.2882 [physics.ins-det].

[16] K. H. Ackermann *et al.* (GERDA), Eur. Phys. J. **C73**, 2330 (2013), arXiv:1212.4067 [physics.ins-det].

[17] (2015), NIRONIT Edelstahlhandel GmbH & Co. KG, Eckeler Strasse 10, D-21224 Rosengarten, Germany.

[18] W. Maneschg, M. Laubenstein, D. Budjas, W. Hampel, G. Heusser, K. T. Knopfle, B. Schwingenheuer, and H. Simgen, Nucl. Instrum. Meth. **A593**, 448 (2008).

[19] Boiler and Pressure Vessel Committee, *ASME boiler and pressure vessel code, Section VIII, Division 1* (American Society of Mechanical Engineers, Two Park Avenue New York, NY 10016-59905, 2015).

[20] (2015), Seismic Design Maps & Tools, United States Geological Survey, 12201 Sunrise Valley Dr, Reston, VA 20192-0003.

[21] B. K. Tsai, D. W. Allen, L. M. Hanssen, B. Wilthan, and J. Zeng, in *Reflection, Scattering, and Diffraction from Surfaces, 11-12 August 2008, San Diego, California, USA*, Proc. SPIE, Vol. **7065** (2008) p. 70650Y, *A comparison of optical properties between high density and low density sintered PTFE*.